CONF-960340--1

LA-UR- 96- 746

LA-UR-

Title: Modeling Ductile Dynamic Fracture with ABAQUS/ Explicit

Author(s): Charles A. Anderson, Los Alamos National Laboratory
Cameron Turner, University of Wyoming

Submitted to: ABAQUS Users' Conference
Newport, RI
May 29 - 31, 1996

Los Alamos
NATIONAL LABORATORY

Modeling Ductile Dynamic Fracture with ABAQUS/Explicit

Charles A. Anderson
Los Alamos National Laboratory

Cameron Turner
University of Wyoming

ABSTRACT

This paper illustrates the use of advanced constitutive models in ABAQUS/Explicit together with highly focused finite element meshes to simulate the propagation of a fracture in a ductile medium. A double edge-cracked specimen under far field dynamic tensile loading is analyzed, and shows both rectilinear motion or unstable oscillatory motion of the crack depending on the material property constraints. Results are also presented for a simulation of ASTM's standard fracture test E399. Comparisons of ABAQUS/Explicit results with experiments or other analytical/numerical results are made.

INTRODUCTION

Dynamic fracture mechanics is concerned with the description of the mechanical state of a deformable body containing a crack, with a view of characterizing the resistance of a material to crack growth taking into account the effects of material inertia and strain-rate. Numerical simulation of dynamic fracture is currently an evolving capability-one which is important to national defense programs, to aerospace structural safety, and to understanding fracture mechanics experiments that are ongoing. Experiments generally show that the crack propagation velocity, V_c, is determined by microcrack interaction and void nucleation and growth ahead of the crack tip with the upper limit to the crack velocity being the Rayleigh surface wave velocity (~2.9 mm/μsec for steel). The features of ABAQUS/Explicit that we use in our numerical simulations of ductile fracture dynamics are the Gurson (1977) theory of plasticity for materials with a dilute

concentration of voids, a void nucleation and coalescence feature, as well as rate effects and thermal softening. In the paper we will illustrate the use of the above ABAQUS features together with highly refined finite element meshes to predict the ductile fracture behavior of a double edge-cracked steel specimen under a far field dynamic tensile load. The problem is modeled as 2-D plane strain. Crack propagation velocity is predicted and the stability of the propagating crack (i.e., its propensity to wander away from mode 1 behavior) will be discussed, and comparisons will be made to other numerical or semi-analytical solutions to this problem (Needleman, 1991; Xia, 1995).

Results will also be shown for a simulation of ASTM's standard fracture test E399. This test is a dynamically loaded three point bend test with the loading provided by a hydraulic ram. Prior to loading, the specimen is notched and has a fatigue crack introduced into the specimen at the apex of the notch. As the load is applied, a displacement gage placed across the mouth of the notch records the opening of the notch. Based on this data and a knowledge of the geometry and loading of the ram, the fracture toughness can be determined. The ABAQUS features described previously together with a fine mesh near the crack are used in this simulation. The results of the simulation are then used to calculate the fracture toughness.

DOUBLE EDGE-CRACKED SPECIMEN

Needleman and Tvergaard (1991) numerically analyzed dynamic crack growth of a plane strain double edge-cracked specimen subjected to symmetric impulsive loading at the two ends. The specimen geometry is shown in Fig. 1. We analyzed this problem using ABAQUS/Explicit together with the same finite element mesh in the crack propagation region that was used by Needleman and Tvergaard. The elements in the crack region are 0.0214 mm by 0.0175 mm compared to the crack specimen dimensions of 200 mm by 400 mm. This is a very fine mesh, which is required to obtain accurate crack propagation velocities. Figure 2a illustrates the fine mesh comprising 280 elements in front of the crack while Fig. 2b illustrates how the fine mesh

propagates to the large elements that describe the entire mesh representing one quarter of the specimen geometry. The mesh was generated using the PATRAN code; the total number of CPE4R elements was 5468. Needleman and Tvergaard used as material behavior that described by Gurson (1977) for an elastic-plastic metal that accounts for ductile fracture by nucleation and growth of voids to coalescence. Thus, there are no ad hoc assumptions regarding an appropriate dynamic crack growth criterion. Strain rate, adiabatic heating, and thermal softening effects are included in the Needleman-Tvergaard analysis, and all of the parameters for the analysis are specified in their paper. All of these capabilities are resident in ABAQUS/Explicit in one form or another except that Needleman-Tvergaard used two populations of particles for nucleation and growth to coalescence - these are large inclusions with low strength that result in large voids at an early stage near the crack tip and small particles which require large strains before cavities nucleate. In ABAQUS we use only one set of particles. We fit the various properties that represent the ABAQUS/Explicit input to the Needleman and Tvergaard paper as closely as possible. Table I lists the ABAQUS/Explicit input representing the high strength steel material model for our crack propagation simulations. Stress units are MPa.

The boundary conditions were symmetry conditions to the right of the crack tip along the bottom and along the right hand boundaries of Fig. 2b, no applied tractions on the left hand boundary and along the bottom to the left of the crack tip, and a specified upward velocity on the top boundary. The velocity ramped from 0 to 0.020 mm/ μsec in 10 μsec and was held constant thereafter.

In our first simulation the Gurson model and the void nucleation and growth model were confined to the 280 elements of the fine mesh region to the right of the crack tip, while the rate dependent/standard plasticity model was used outside of the fine mesh region. Figure 3 illustrates the position of the crack tip as a function of time when the double edge-cracked specimen has been

subjected to the impulsive tensile loading at its ends and using the material properties for high strength steel and a void tensile failure strain of 0.25 in the fine mesh region of the specimen shown in Fig. 2a. The crack velocity for this case is clearly seen to be 1.11 mm/μs. If the Gurson plasticity model and the void model are not confined to the fine mesh region but apply to the entire mesh, then a different crack trajectory is produced in which the crack deviates from rectilinear motion and oscillates about the specimen mid-plane as shown in Fig. 4. This result seems to corroborate conclusions about dynamic crack instabilities that were presented by J. S. Langer (1995) at a recent symposium held at Los Alamos.

Our simulation study shows a different behavior than that of Needleman and Tvergaard in that their analysis indicated a crack propagation velocity of 0.651 mm/ μsec and did not exhibit oscillatory behavior. The difference in velocity can probably be attributed to the difference in particle distributions in the two analyses.

ASTM STANDARD FRACTURE TEST

The American Society of Testing and Materials (ASTM) Test E399 is one of a number of tests designed to determine the fracture toughness of a material in a dynamic loading situation. Test data exist for several common materials, most often at or below room temperature. We selected 6061-T6 as our model material since fracture toughness data do exist for this material at room temperature.

Figure 5 is a schematic of the dynamic fracture test that we modeled using ABAQUS/Explicit. Basically the test is a dynamically loaded three point bend test with a linear increasing loading provided by a hydraulic ram. Prior to loading, the specimen is notched and a fatigue crack is introduced into the specimen at the root of the notch. A displacement gage placed across the mouth of the notch records the opening of the notch during the test. Various conditions must apply to obtain a valid test; these are described in Reference 1.

Figure 6 illustrates the mesh, comprising about 40,000 nodes and plane strain elements, that we used to model the fracture test. Symmetry boundary conditions were used to reduce the problem to one-half of the test configuration. A contact surface was set up between the ram and the test specimen. As in the previous calculation we used a highly refined mesh in the region of the test specimen where the crack would propagate. The Gurson model was taken for all elements in the test specimen while the high strength loading ram was assumed to exhibit conventional elastic-plastic behavior. Material properties for ram and specimen that were used in the calculation are listed in Table II.

The example calculation was executed with a loading rate of 5833 kN/s applied to the ram. After the conclusion of the example calculation, data were extracted for critical elements that would be located along the anticipated crack path, and for nodes whose displacement measured the ram motion and the crack opening. The data were used to generate the load displacement curve shown in Fig. 7. The 95% secant curve was also calculated based on the slope between the second through the fifth time intervals. This curve was used later to calculate a fracture toughness for the material.

In the data from the example calculation there was seen to be four regions of crack tip behavior as shown in Fig. 8. The first region, where the crack does not propagate, ends after about 450 μs. During this initial loading, a dynamic stress concentrations develops gradually around the crack tip. When the volumetric strain in the first element ahead of the crack tip reaches 0.25, the element fails according to the Gurson model.

In region 2, denoted by a velocity spike at 450 μs, the crack propagation occurs as an explosive burst. The detailed view of the volumetric strain around the crack tip is shown in Fig. 9, and indicates that there are three separate cracks that have appeared from the stress concentration

ahead of the crack tip. This is characteristic of unsteady crack propagation. These cracks coalesce back into a single crack within a few μs and a more stable region of crack propagation appears.

After the three crack tips have coalesced into a single crack, a region of stable crack propagation exists until approximately 550 μs. In this region, the primary failure mechanism of the specimen is crack propagation. The stable nature of the crack propagation makes this region ideal for the determination of the critical stress intensity. The volumetric strain around the crack for this region of behavior is shown in Fig. 10.

By 550 μs, the stable region of crack propagation has given way to a region that is influenced by other failure mechanisms. The crack tip velocity profile is no longer constant, but seems to have a more periodic behavior. This behavior is the result of plastic waves, caused by the approaching ram, interrupting the propagation of the crack tip. Figure 11 illustrates the tensile volumetric strain at 850 μs, well into region 4 behavior.

Further details of this analysis, as well as the calculation of the fracture toughness, which agreed closely with experimental values, are given in Turner, 1995.

REFERENCES

1. ASTM Standards, Vol. 3.01, "Standard Test Method for Plain-Strain Fracture Toughness of Metallic Materials," pp 509-539, 1993.
2. Gurson, A. L., "Continuum Theory of Ductile Rupture by Void Nucleation and Growth: Part I - Yield Criteria and Flow Rules for Porous Ductile Media," J. Engng. Mater. Technology 99, pp 2-15, 1977.
3. Langer, J. S., "Dynamic Instabilities in Fracture," Presentation at the Fractal Analysis and Modeling of Materials Workshop, April 26-27, 1995, Los Alamos, NM.

Table II. Model Material Properties Used in ASTM Fracture Test Simulation

Material Property	Plate (A1-6061-T6)	Loading Ram (Steel)
Density (kg/m3)	2,710	7,800
Young's Modulus (MPa)	70,000	200,00
Poisson's Ratio	0.3	0.3
Yield Strength (MPa)	240	300
Failure Criteria	Gurson Model - 25% volumetric strain	Conventional

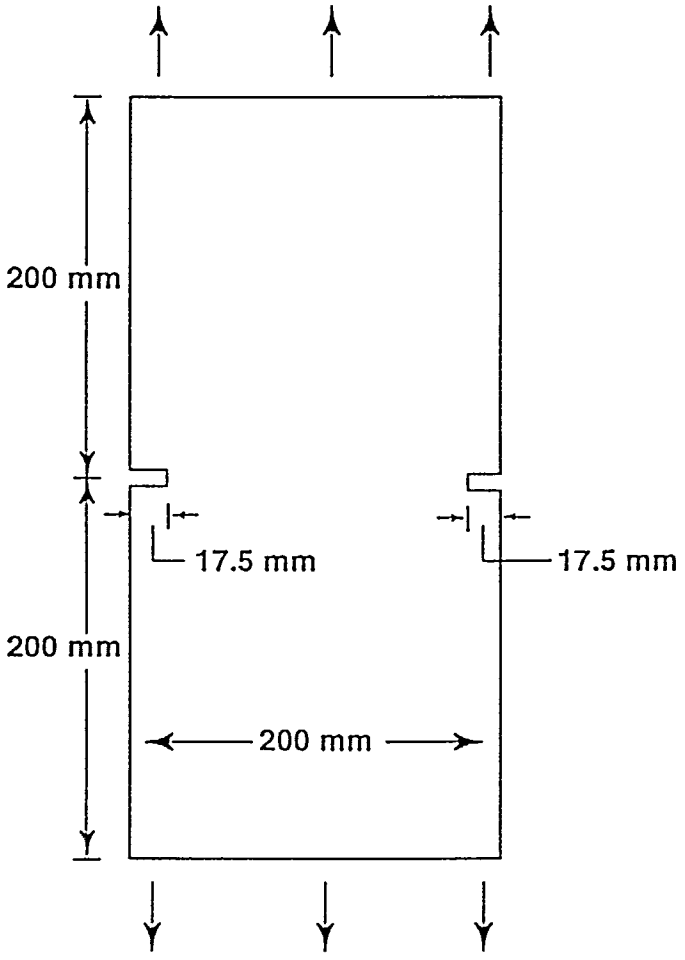

Fig. 1. Geometry of double edge-cracked specimen.

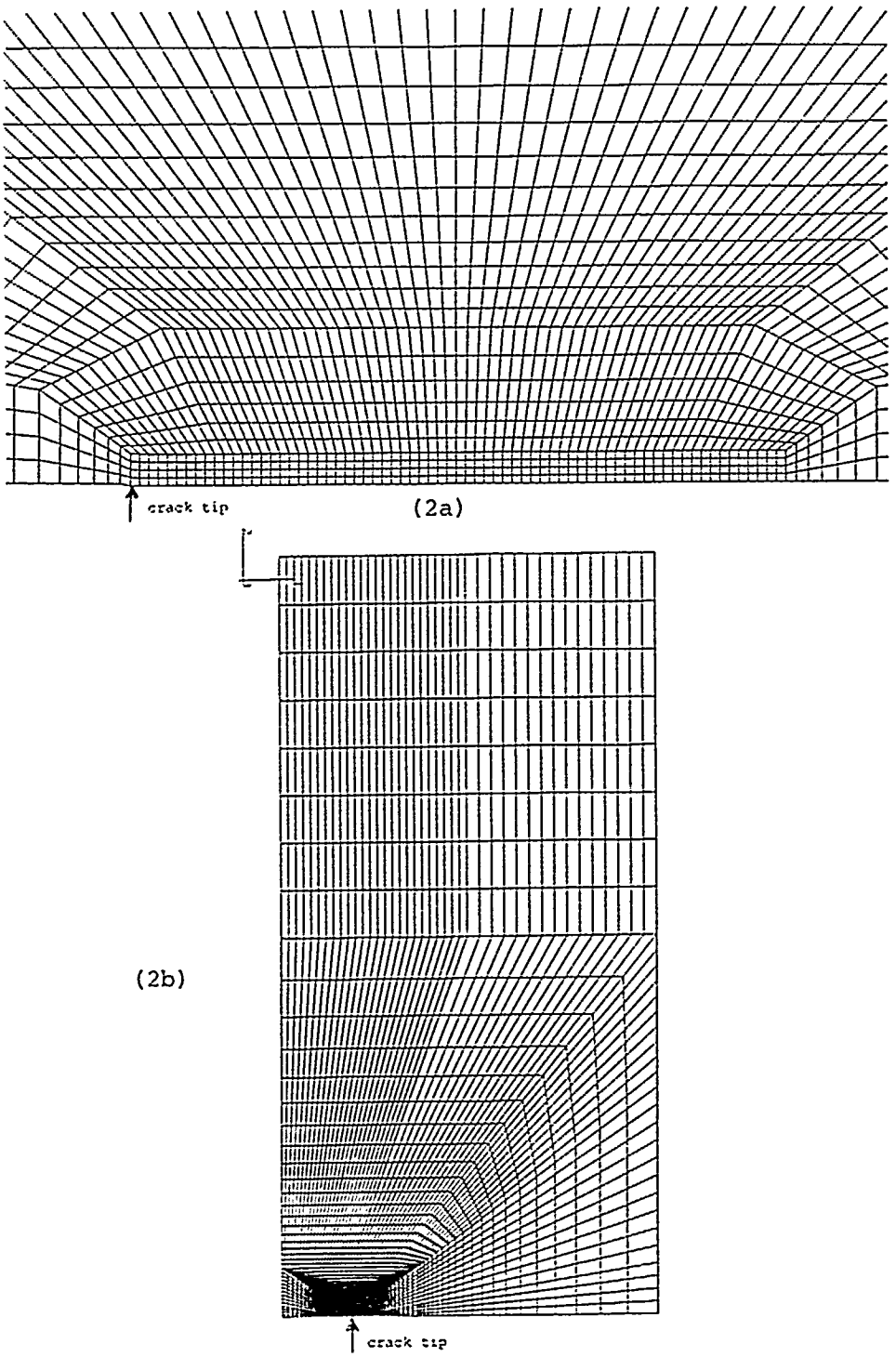

Fig. 2. Finite element crack tip mesh for a double edge-cracked specimen showing transition from a fine mesh at the crack tip (2a) to a much coarser global mesh (2b). A uniform grid of the fineness at the crack tip would require over 50 million elements.

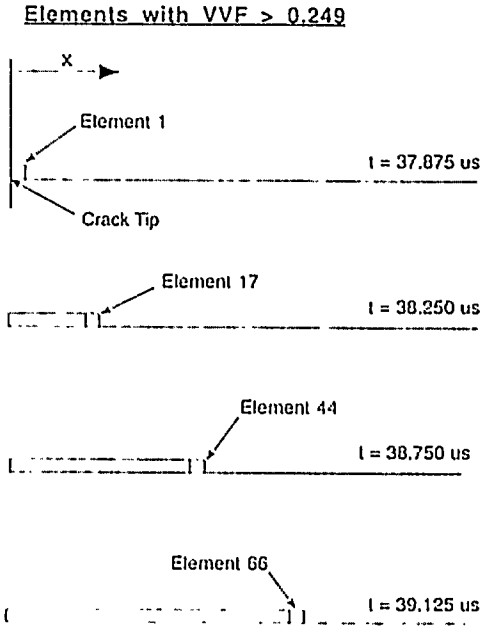

Fig. 3. Crack tip displacement data and linear fit.

CRACK PROPAGATION DATA (from tip6 run)	
Time (us)	Distance x (mm)
37.875	0.021
38.000	0.129
38.125	0.257
38.250	0.364
38.375	0.514
38.500	0.643
38.625	0.793
38.750	0.943
38.875	1.093
39.000	1.221
39.125	1.414

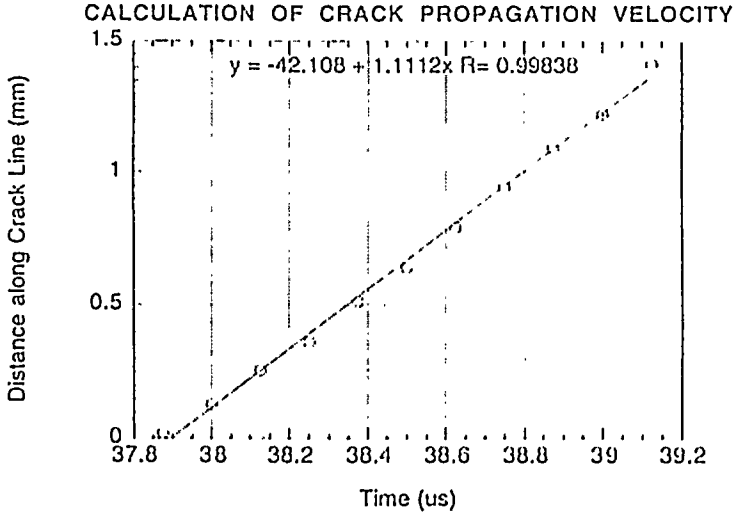

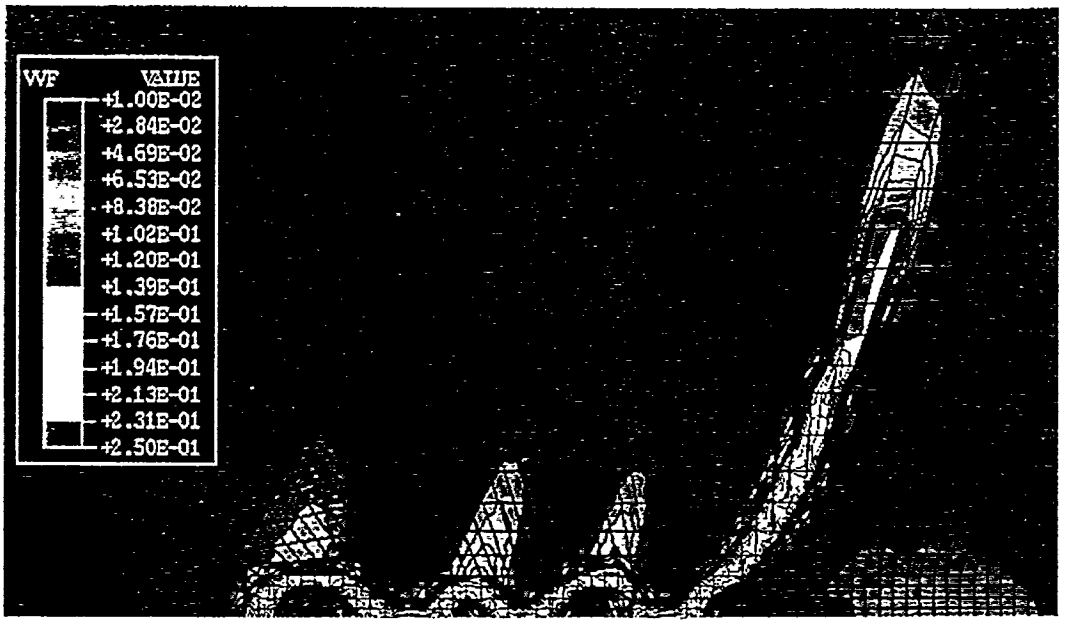

Fig. 4. Unstable crack propagation, crack propagation velocity ≅0.6 mm/μs.

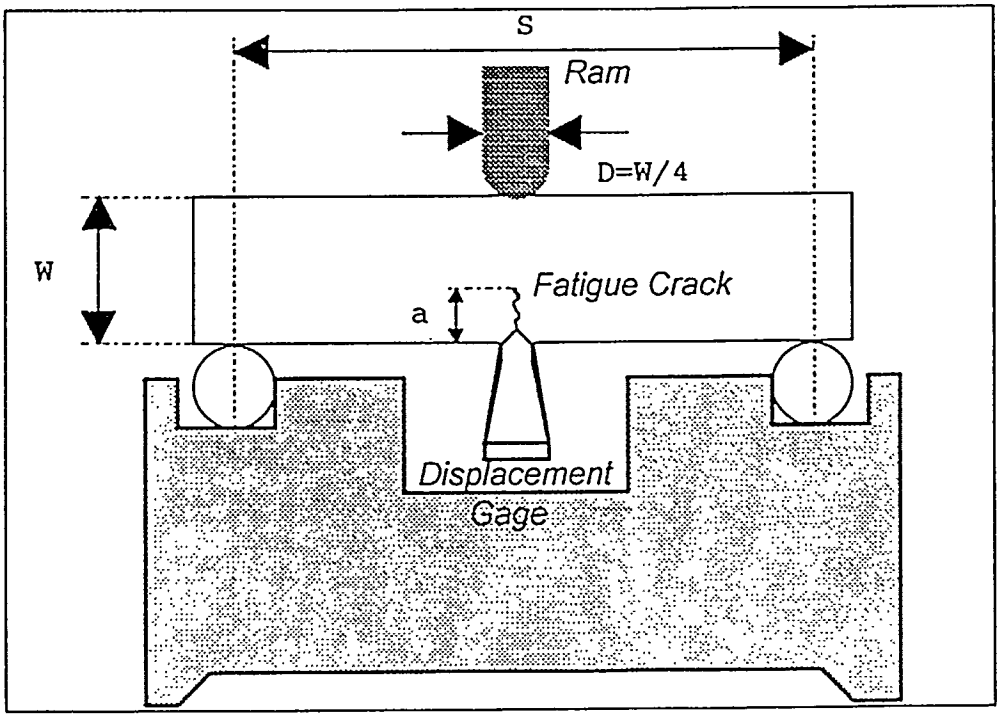

Fig. 5. Schematic of dynamic fracture test setup.

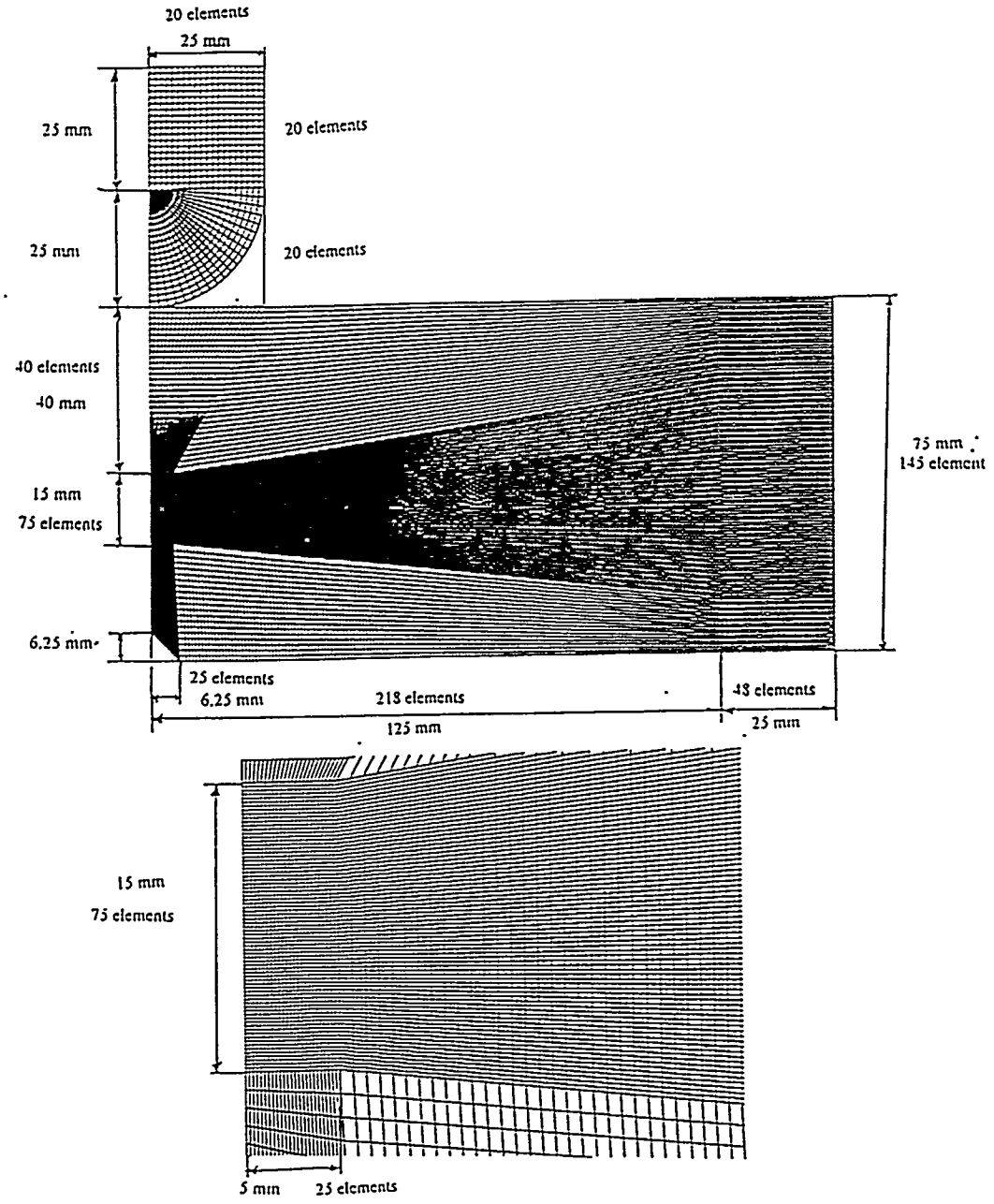

Fig. 6. Finite element mesh showing fine mesh region for dynamic fracture test.

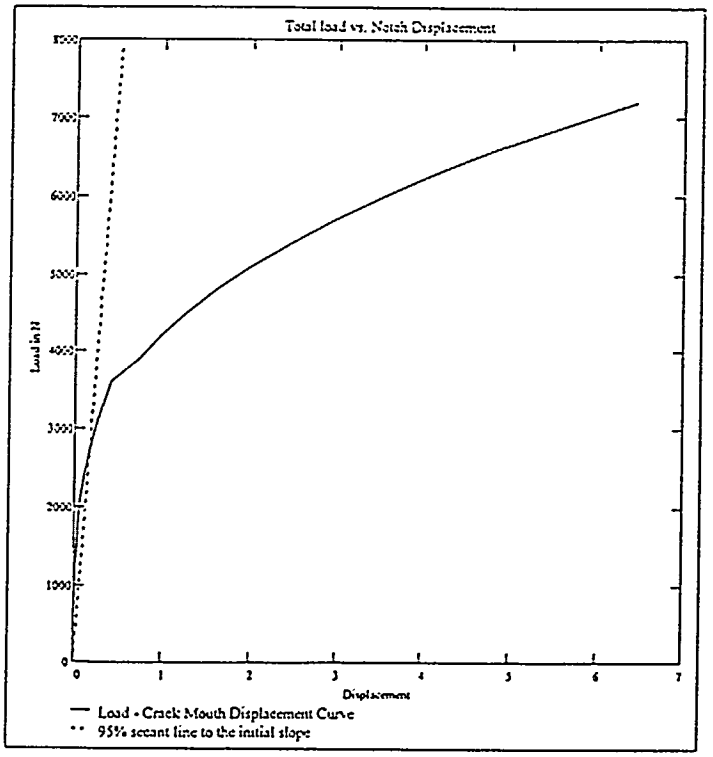

Fig. 7. Load vs. crack opening displacement showing 95% secant intercept.

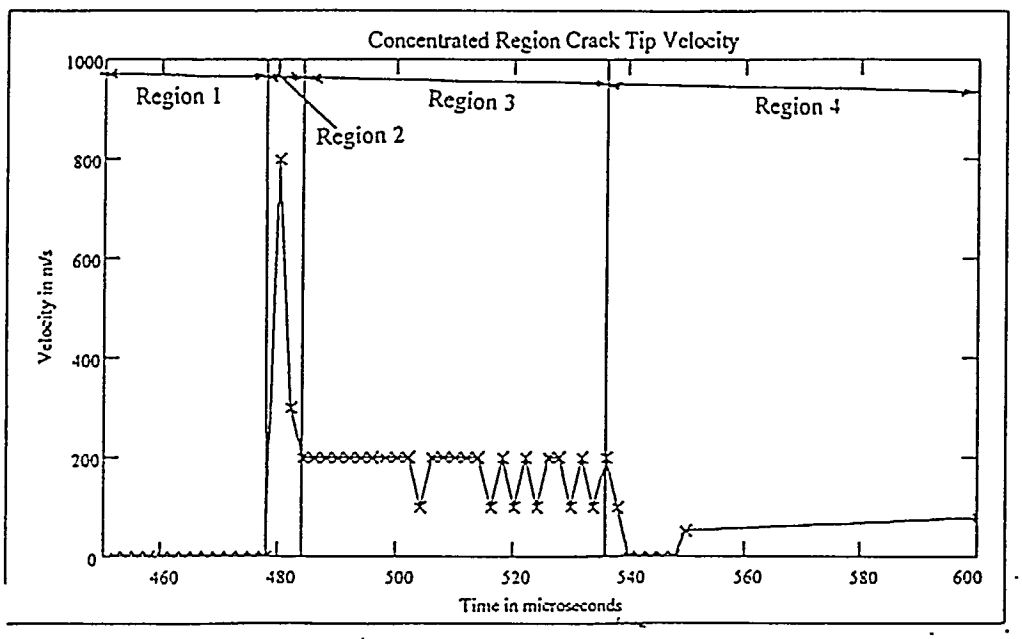

Fig. 8. Crack tip velocity as a function of time during fracture showing the 4 crack behavior regions.

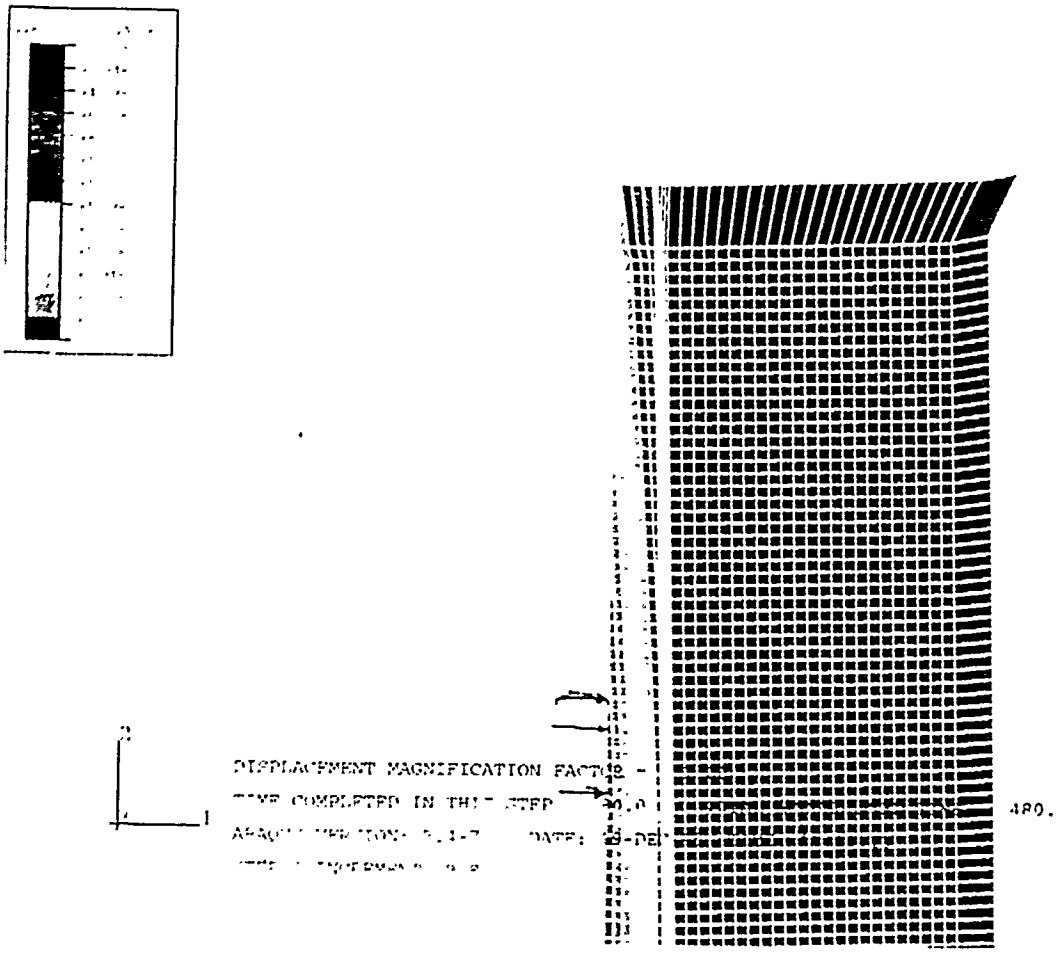

Fig. 9. Volumetric tensile strain field at 480 μsec.

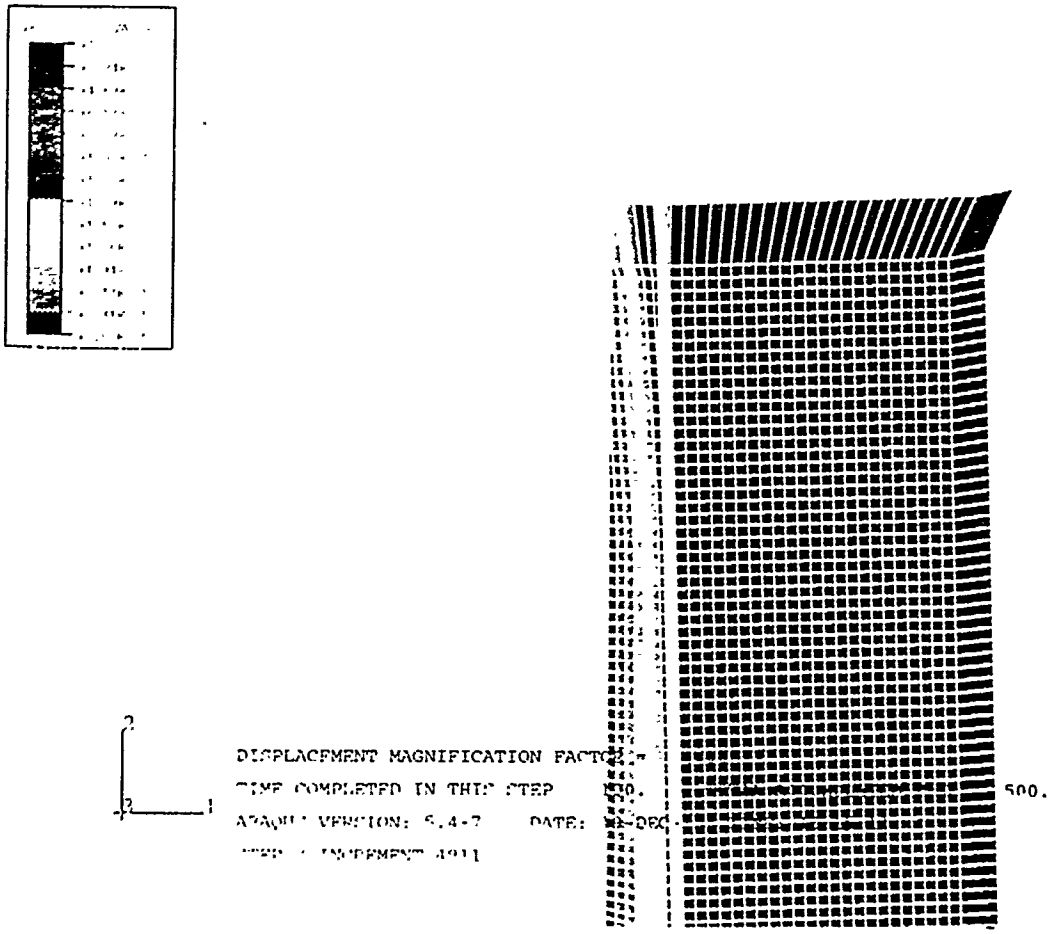

Fig. 10. Volumetric tensile strain field at 500 μsec.

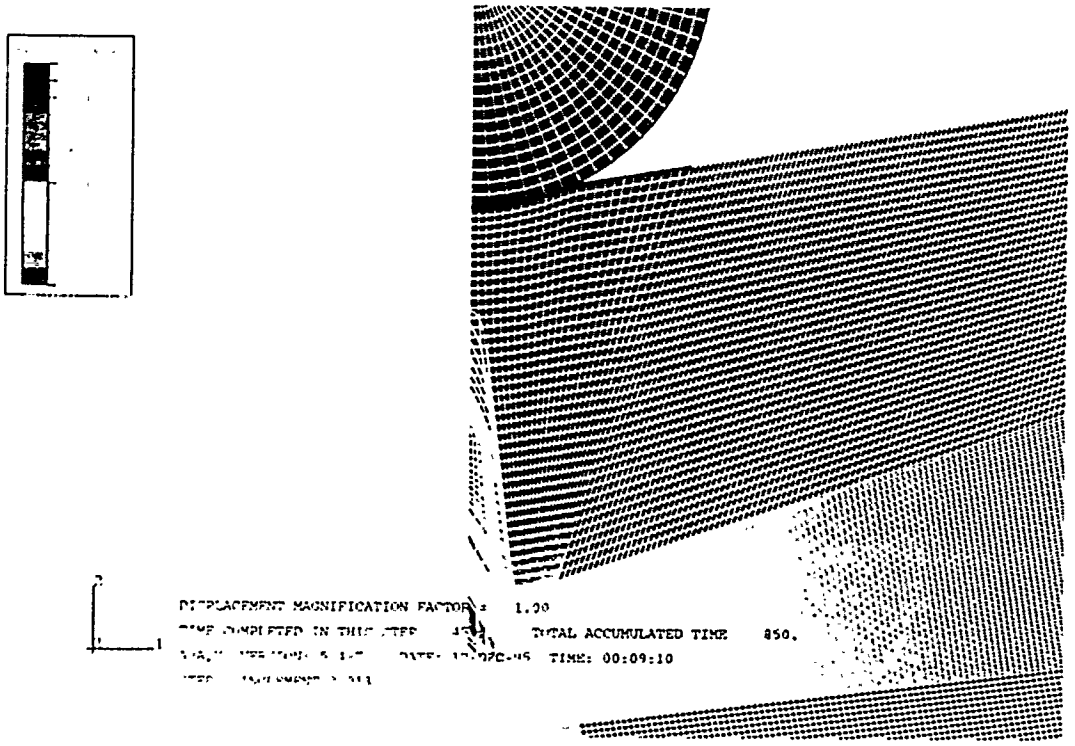

Fig. 11. Volumetric tensile strain field at 850 μsec showing complete rupture of the fracture test specimen.